Beam Tracking Based on a New State Model for mmWave V2I Communication on 3D Roads

Yu Sun, Chen-Wei Feng[*], Xian-Ling Wang, Jiang-Nan Yuan, Lin Zhang

School of Opto-electronic and Communication Engineering, Xiamen University of Technology,
Xiamen, Fujian, China

978995028@qq.com, cwfeng@xmut.edu.cn, xianling.wang@ieee.org,
jnyuan@xmut.edu.cn, 2010110609@xmut.edu.cn

Abstract. The expansion of 5G and Internet of Things has laid a good foundation for the in-depth research of Internet of vehicles. Low frequency resources are scarce, and Internet of vehicles communication requires extremely high communication rate. Millimeter wave can meet the above two requirements, but its characteristics and the complicated communication conditions of Internet of vehicles make it difficult to combine the two. Overcoming these problems and making beam tracking accurate and steady is a major challenge at present. In this paper, a new extended Kalman filter tracking algorithm is proposed for mmWave V2I scenarios. On the basis of the original algorithm, a threshold prediction update mechanism is added. A new scheme is adopted, which takes position and velocity as tracking variables, and the tracking model is derived for the first time in MIMO 3D scenarios based on this scheme. The model considers the three-dimensional road conditions, including the vehicle deflection motion and the millimeter wave link blocked by large vehicles, which is more suitable for practical application scenarios. The simulation results reveal that the position and velocity tracking scheme is superior to the angle and gain tracking scheme, and the tracking error of the proposed algorithm is lower than that of the algorithms using similar state models. Based on the three-dimensional scene, it considers more realistic situations, and is more consistent with the kinematic characteristics of the vehicle and has more practical significance.

Keywords: multiple-input multiple-output, beam tracking, extended Kalman filter, internet of vehicles, millimeter wave

1 Introduction

With the increasing of vehicle ownership, the carrying capacity of urban roads tends to be saturated, and the problems of traffic safety and travel efficiency become more and more prominent. With the expansion of Internet of Things (IoT) technology and continuous growth of car ownership, domestic and international scholars have drawn extensive attention to Internet of Vehicles (IoV). IoV links vehicles, networks and transportation facilities in the scene, effectively improving information interaction. Its core technology is Vehicle to Everything. With rich spectrum resources and high data rate, millimeter wave is very consistent with the needs of the IoV scenario, so it has become one of the powerful candidate technologies for the communication medium of the future IoV architecture [1, 2].

However, adverse effects of mmWave and complicated conditions of IoV have imposed many restrictions on the architecture of mmWave IoV [3-5]. Different from low-frequency signals, mmWave communication will produce higher propagation losses. The atmosphere and rain will also absorb mmWave signals, which further reduces the communication range of mmWave. Fortunately, mmWave small size antennas can construct Multiple Input Multiple Output (MIMO) antenna arrays, which can form directional beams through beamforming technology. This beam has strong directivity and high gain coefficient, which can offset the high transmission loss of mmWave to a certain extent. In addition, mmWave cannot penetrate most solid materials, and its transmission signal can only be transmitted at the Light of Sight (LOS). In the scenario of high mobility IoV, traffic connections are readily interrupted by obstructions, for instance, other vehicles and constructions. The high mobility of users in IoV scenarios will cause serious Doppler shift and frequent channel changes, which reduces the reliability of transmission. Vehicle users in the IoV scenario need low communication delay under high speed movement. If the above problems cannot be properly overcome, the security of automatic driving and other functions will be

---

* Corresponding Author

greatly reduced due to frequent link disconnection, and the frequent channel estimation will generate huge overhead. Therefore, ensuring the continuity and accuracy of communication links requires beam tracking to reduce the probability of link disconnection and ensure effective communication.

The complex time-varying channel conditions of high-speed vehicle movement and the NLOS transmission and strong directivity characteristics of mmWave should be considered simultaneously in the research of mmWave IoV. Under the combined influence of the above conditions, it is one of the major challenges to implement accurate and steady beam tracking and guaranteed communication.

For a user who is moving at high speed, a training beam is sent during the communication to allow accurate tracking of its changing channel. Such data transmission scheme used to deal with such users with high mobility is usually called beam tracking [6-8]. Since the high directionality of the beam in mmWave MIMO system, the communication parties are easy to suffer from beam misalignment and communication interruption due to small device movement or environmental changes. Especially in the environment where the channel changes rapidly, frequent beam misalignment is easy to cause frequent beam access. Therefore, efficient beam tracking method is very important for mmWave communication in dynamic scenarios.

Beam tracking in millimeter wave communication can be generally divided into three categories [9-11]: (1) Beam tracking based on training; (2) Beam tracking based on dynamic filtering principle; (3) Beam tracking based on sensor fusion. Training-based beam tracking maintains beam alignment by regularly training the beam direction, which requires a high enough training frequency to cope with fast channel changes, so the system overhead is high. In beam tracking based on sensor fusion, various sensors (such as GPS) are generally used to sense the position information to assist tracking. However, for small communication devices with limited load and power consumption, this method has great limitations. In contrast, beam tracking based on dynamic filtering principle mainly uses iterative prediction method, which has less overhead and less limitations. However, it is easy to be affected by environmental mutation, and the tracking error will accumulate over time. This is also the tracking method that this paper focuses on.

Some commonly used filtering algorithms for dynamic systems are Kalman Filter (KF), Unscented Kalman Filter (UKF), Extended Kalman Filter (EKF), and Particle Filter (PF) [10], etc. These filter algorithms generally build the status model, and then estimate the state of the system in a discrete interval through the observation model to achieve the purpose of state tracking.

The filtering scheme based on EKF is proposed in [12-15]. Reference [12] proposed an EKF filtering tracking algorithm based on second order Taylor expansion. This algorithm chooses the second order expansion instead of using the general first order expansion. In the case of improving the computational complexity and sacrificing part of the delay, the beam tracking accuracy is improved. The subsequent experiments show that the mean square error (MSE) performance of the proposed algorithm is superior to the original EKF algorithm and PF algorithm without increasing the computational complexity. All possible beam combinations are comprehensively scanned in [13], which is used to create the measurement matrix applied in EKF filtering. This method requires high pilot overhead to obtain the measurement matrix. This makes it difficult to take long measurements and track a rapidly changing environment. Moreover, the state model is based only on the angle and does not consider the path gain. In [14], angle changes are tracked by a single measurement instead of the whole scan, thus reducing the overall overhead. Although the scheme of [14] reduces the number of beam scanning to a certain extent, for a highly nonlinear tracking system, the operation of EKF using the Jacobian matrix linearization system is more complex, and the dynamic tracking performance is slightly poor. Reference [15] proposes a robust beam tracking strategy, which combines iterative optimization MSE and EKF principle, to solve the problem that the received signal quality drops sharply due to the angular deviation of the receiving and transmitting beams in the mobile mmWave communication scene. The algorithm uses EKF filter to track the angle and antenna gain, and then smoothed the tracking error based on the MMSE criterion to eliminate linearization error introduced by EKF linear approximation and reduce the beam tracking error in mobile environment.

Reference [16, 17] carried out research work based on UKF. Reference [16] uses UKF to track the path angle and gain information in the channel. In [17], linear Gauss-Markov process was used to model the dynamic status space of the millimeter wave channel, and the beamformer based on UKF was designed. Theory and simulation verify that UKF can effectively bring better estimates than EKF given the initial channel estimates. However, the abnormal disturbance of the system makes the UKF tracking algorithm difficult to converge and affects the beam tracking process. A beam tracking method using PF is proposed in [18] to improve the tracking accuracy. Although the particle filter has high tracking accuracy, it brings huge system overhead and tracking time, so it is not suitable for beam tracking in the dynamic millimeter wave channel.

Most of the above papers adopt millimeter wave beam tracking model with tracking angle and gain. Reference [19] argues that the current status tracking model is unsuitable for millimeter wave vehicle communication. The

state model has nonlinear and non-additive noise, and the motion characteristics of the vehicle cannot be considered. It proves this point of view through calculation. It is shown that if angle is used as a state variable, the calculation of Jacobian matrix of EKF algorithm becomes very complicated and impractical. During the tracking process, the amount of angle change is nonlinear with respect to the angle, and since the assumed noise generated by the speed change is nonadditive, using angle as a state variable will greatly increase the computational complexity of the Jacobi matrix of the EKF algorithm. Therefore, the use of vehicle position and speed as state variables is more suitable for V2I communication scenarios, but there are still some limitations in the study of this model due to the difficulty of research. Therefore, this paper constructs a tracking model using position, speed and gain, and provides linear status models and additional noise suitable for this model. Verification shows that this method considers vehicle motion characteristics and improves beam tracking with lower complexity. However, this scheme is only based on the two-dimensional scene under MIMO, which is not in line with the actual application scenario. Reference [20] constructed a 3D scene model with position and speed as tracking variables, and used uplink detection signals to feed a small amount of vehicle information back to Road Side Unit (RSU) to predict the vehicle motion state in high mobility scenarios. Although 3D scene is discussed in this paper, considering the complexity, only MISO scene is discussed, which has certain limitations.

According to the above shortcomings, this paper carries out further research. The contributions of this paper are listed below:

(1) Using position and velocity as the state model for tracking is undoubtedly a relatively new way. However, as mentioned above, the current research on this tracking model still has limitations. In this paper, with position and velocity as the tracking variables, combined with the antenna model of MIMO, the beam tracking model in the 3D road scenario is derived.

(2) To be more consistent with actual scenarios and make researches more general, more realistic situations are considered. This paper considers the problem that communication links may be blocked by large vehicles in reality, and establishes a two-dimensional occlusion model to provide a simple solution. The angle deflection factor existing in the vehicle driving process is considered, which is more consistent with the actual motion of the vehicle in the 3D scene.

(3) The beam tracking procedure suitable for the new scheme in this paper is designed. An EKF beam tracking algorithm for mmWave V2I is proposed. In this procedure, better tracking performance can be obtained with lower overhead. The threshold prediction update method is used to limit the accumulated errors in the EKF algorithm, and the state information fed back to the RSU is used for one-step prediction. The accumulated tracking errors are updated iteratively to enhance the accuracy of the algorithm and increase the effective tracking time.

The remainder of this paper is organized as follows. In Section 2, the system model is introduced. The scene is established, the scheme to suppress the occlusion effect is obtained by 2D modeling, and the transmission model is constructed. In Section 3, a new beam tracking procedure is designed, and the threshold prediction updated EKF algorithm based on the new state model is derived. In Section 4, the scheme is compared with other algorithms and its performance under different conditions is studied. Section 5 summarizes the full paper.

Notation: $\mathbf{A}$ represents a matrix, $\mathbf{a}$ denotes a vector and a is a scalar. $\mathbf{A}^{\mathrm{T}}$, $\mathbf{A}^{*}$, $\mathbf{A}^{\mathrm{H}}$, $\mathbf{A}^{-1}$ and $\|\mathbf{A}\|^2$ respectively denotes the transpose, conjugate, conjugate transpose, inverse and magnitude of $\mathbf{A}$. $|a|$ denotes the absolute value of a . $E[\bullet]$ is the expected value. $\mathbf{I}_M$ is the $M \times M$ identity matrix. $\mathcal{CN}(m, \sigma^2)$ means complex Gaussian random variable with mean of m and covariance of σ^2.

2 System Model

2.1 Scenario Model

The scenario is assumed to be a one-way road with two lanes under the architecture of mmWave IoV, and the scenario model is shown in Fig. 1. This road segment is continuously covered by a single RSU, which can communicate with multiple vehicle users at the same time within the coverage area.

To offset the high path loss of millimeter wave, MIMO arrays are set up for both RSU and vehicles. High gain directional beams can be generated by beamforming suitable for MIMO. Among them, the small-size millimeter wave antenna of the vehicle is placed on the top of the vehicle, which can obtain a larger signal receiving and transmitting range and reduce the occlusion problem caused by millimeter wave to a certain extent. After establishing the communication link between RSU and the vehicle, the beam tracking is carried out continuously in the downlink to ensure the stability of the communication link. The vehicle broadcasts state information such as

its position, speed and safety status to the range periodically. After obtaining the state information about the user, RSU can predict the user's motion trajectory based on it, which further guarantees the steady beam tracking. In this case, if the link is disconnected due to an emergency, the channel can be re-estimated based on the information of the last moment to re-establish the link.
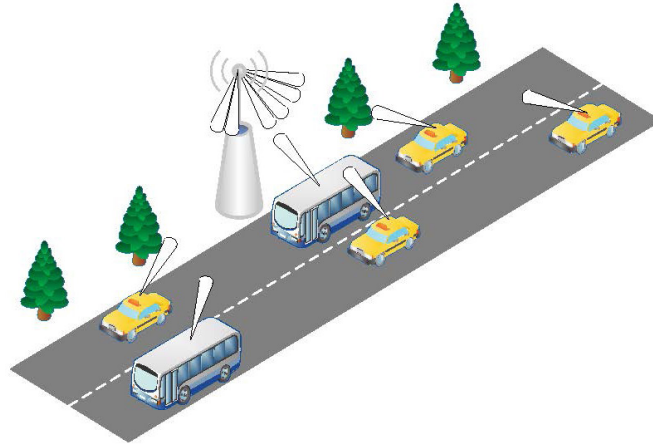
Fig. 1. Scenario model

2.2 Occlusion Problem Suppression

Millimeter waves have blocking properties. It cannot penetrate most solid materials and can only transmit at LOS in most cases. In the actual road scenario, there may be a problem that large vehicles block the mmWave link of small vehicles traveling in the periphery due to the high height. To overcome this problem to a certain extent, a reasonable RSU height can be designed to avoid the occlusion caused by large vehicles. The simple plane occlusion model can be built to calculate the height to be set for the RSU, as shown in Fig. 2.
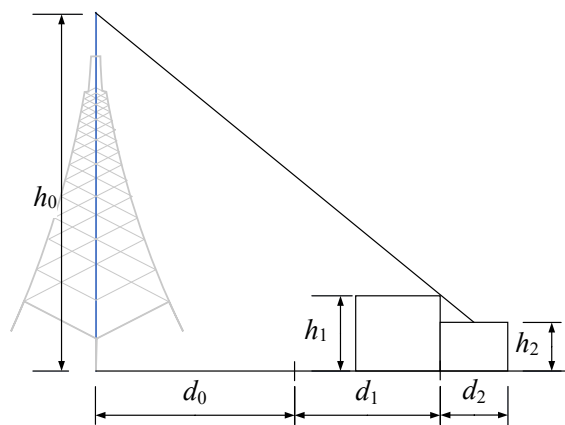
Fig. 2. Plane geometric occlusion model

The 2D plane in the figure adopts the position with the smallest distance between large and small vehicles and RSU. In this case, the required RSU height is the highest in the RSU coverage area. The MIMO antenna used for

receiving and transmitting signals is placed in the center of the roof of the vehicle. To calculate the limit RSU height needed to achieve line-of-sight transmission, the position of the two vehicles close to each other is used for calculation.

RSU height is denoted as h_0. The distance between RSU and road is set as d_0. The lane width is set as d_1. The height of the large vehicle is set as h_1. The height and width of the small vehicle are respectively set as h_2 and d_2. According to the principle of triangle geometry, the relation is:

$$\frac{h_1 - h_2}{d_2/2} = \frac{h_0 - h_2}{d_0 + d_1 + d_2/2} . \tag{1}$$

According to the size of vehicles in real life, d_1 is generally 3.75 meters, d_2 is generally 2 meters, h_1 is generally 3 meters, h_2 is generally 1.5 meters. Based on this assumption, it can be further calculated that:

$$h_0 = 1.5d_0 + 8.625 . \tag{2}$$

Only when the RSU is high enough, the mmWave link is not easily occluded. However, due to the limit of height and high path loss of mmWave, RSU should not be designed too high. Therefore, the design of RSU height needs to select the appropriate height according to the above equation, and the RSU can be considered to be placed on the top of the nearby building to reduce the construction cost.

2.3 Transmission Model

This paper focuses on the downlink V2I communication process. Because of the narrow beam, strong directivity and strong anti-jamming ability, the interference between the beams is very small. To simplify the model, the influence of other beams is assumed to be negligible, and the object of study can be reduced to a single RSU communicating with a single vehicle user. The research model is shown in Fig. 3. The coordinate system is constructed with RSU as the origin, the vehicle's forward direction as the x-axis, and the vertical direction of forward direction as the y-axis.
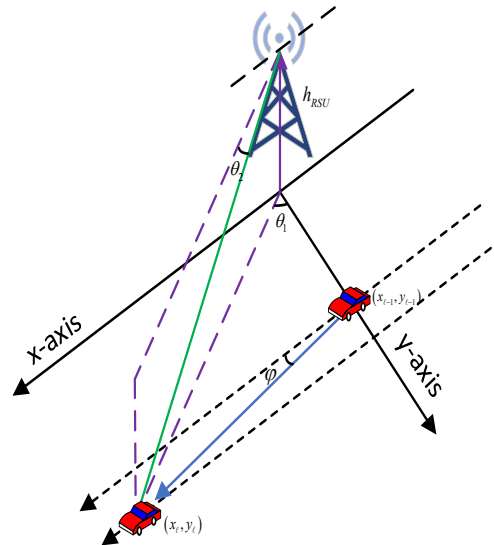
Fig. 3. Research model

Most of the literature on mmWave channel is based on the hybrid precoding framework. Traditional MIMO arrays are usually fully digital. The antenna is assigned with exclusive RF chain, which is relatively expensive [21]. Massive MIMO antenna arrays have a significant number of antennas, which require a significant amount of RF chains. Due to the low cost, analog/digital hybrid architecture with low RF chain number has attracted much attention in the research community. The corresponding signal processing techniques need to be reconstructed for hybrid architectures to achieve great compromise between cost, overhead and transmission efficiency [22]. As mentioned above, MIMO systems can be built on the roof of the cars with the small size mmWave antennas. In this scenario, the hybrid beamforming architecture is applicable to both RSU and vehicular MIMO, and the scheme is displayed in Fig. 4.
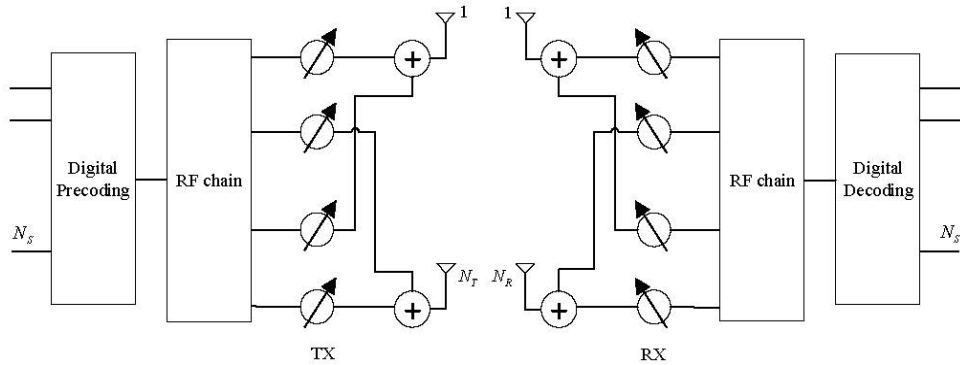
Fig. 4. Hybrid beamforming scheme

Uniform Linear Array (ULA) is applied at both transmitting terminal and receiving terminal to meet the generality. The number of antennas at the receiving terminal is N_R, the number at the transmitting terminal is N_T similarly. Normally, the quantity of RF chain will not be larger than the number of antennas. For simplicity, the scheme is studied only for a single user. Therefore, it is supposed that there is only one RF chain at each node. In accordance with the hybrid beamforming framework, data symbol S is first precoded in baseband and RF through beamforming vector $\mathbf{f}$ at the transmitting terminal, and then received through beammerging vector $\mathbf{w}$ at the receiving terminal after conveying through the system channel. Beamforming vector and beammerging vector satisfy $\|\mathbf{f}\|^2 = 1$ and $\|\mathbf{w}\|^2 = 1$.

Accordingly, the received signal is conveyed as:

$$r_\ell = \sqrt{\rho_\ell}\,\mathbf{w}^{\mathrm{H}}\mathbf{H}_\ell\mathbf{f}\,s + \mathbf{w}^{\mathrm{H}}\mathbf{n}_{\mathrm{AWGN}} = \sqrt{\rho_\ell}\,\mathbf{w}^{\mathrm{H}}\mathbf{H}_\ell\mathbf{f}\,s + n_\ell . \tag{3}$$

Where ρ_ℓ is the average SNR, $\mathbf{H}_\ell$ is the channel matrix, and $\mathbf{n}_{\mathrm{AWGN}}$ is additive complex white Gaussian noise with mean 0. Since $\|\mathbf{w}\|^2 = 1$, n_ℓ obeys the identical element distribution of vector $\mathbf{n}_{\mathrm{AWGN}}$. The average SNR is constructed as:

$$\rho_\ell = \frac{p}{\sigma_n^2}\left(\frac{\lambda}{4\pi d_\ell}\right)^n . \tag{4}$$

Where p represents transmission power, σ_n^2 represents noise power, λ denotes wavelength, d_ℓ denotes the distance between RSU and vehicle, and n is the path loss index.

In addition to strong directivity, mmWave channels also have limited scattering and sparse low rank characteristics. It is generally modeled by Saleh-Valenzuel millimeter wave channel model. To better fit the research scenario of this paper, the influence of multipath is not considered. The time-varying channel model is briefly written that:

$$\mathbf{H}_{\ell} = \mathbf{a}_{R}\left(\theta_{\ell}\right)\beta_{\ell}\mathbf{a}_{T}^{H}\left(\phi_{\ell}\right). \tag{5}$$

According to [23], when ULA is adopted, the antenna array of RSU can be adjusted to be parallel to the forward direction of the vehicle, in which case the Angle of Arrival (AoA) and Angle of Departure (AoD) can be approximately equal, namely $\phi \approx \theta$. According to this conclusion, the subsequent AoA and AoD are represented by ψ.

Then according to the above conclusion, in the channel model of millimeter wave band, the channel matrix may be denoted by function ψ_{ℓ} that controls the beam orientation of the radio propagation path, namely $\mathbf{H}_{\ell} = \mathbf{H}(\psi_{\ell})$. Substituting (5), which is uniformly represented by (ψ_{ℓ}), into (3), the downlink input-output expression at discrete time ℓ is:

$$r_{\ell} = \sqrt{\rho_{\ell}}\mathbf{w}_{\ell}^{H}\left(\mathbf{a}_{R}\left(\psi_{\ell}\right)\beta_{\ell}\mathbf{a}_{T}^{H}\left(\psi_{\ell}\right)\right)\mathbf{f}_{\ell}s + n_{\ell}. \tag{6}$$

Where β_{ℓ} is the channel gain coefficient, $\mathbf{a}_{R}(\psi_{\ell})$, $\mathbf{a}_{T}(\psi_{\ell})$ are the array response vectors.

According to [21], the gain coefficient can be expressed as:

$$\beta_{\ell} = \overline{\beta}d_{\ell}^{-1}e^{j\frac{2\pi}{\lambda}d_{\ell}} = \overline{\beta}d_{\ell}^{-1}e^{j\frac{2\pi f_{c}}{c}d_{\ell}}. \tag{7}$$

Where $\overline{\beta}d_{\ell}^{-1}$ represents the path loss of the channel with distance, $\overline{\beta}$ represents the reference power gain at the distance of 1 meter, and $2\pi d_{\ell} / \lambda$ denotes the phase of the LOS path. Assuming that the RSU knows the reference power gain factor $\overline{\beta}$, estimating the channel gain coefficient β_{ℓ} is equivalent to estimating the distance d_{ℓ}. The tracing model can be further simplified by relying on this conclusion.

The array response vectors of receiving terminal and transmitting terminal are expressed as $\mathbf{a}_{R}(\psi_{\ell})$ and $\mathbf{a}_{T}(\psi_{\ell})$ respectively. Since ULA is adopted, it can be constructed as:

$$\mathbf{a}_{R}\left(\psi_{\ell}\right) = \frac{1}{\sqrt{N_{R}}}\left[1, e^{j\psi_{\ell}}, \cdots, e^{j(N_{R}-1)\psi_{\ell}}\right]^{T}. \tag{8}$$

$$\mathbf{a}_{T}\left(\psi_{\ell}\right) = \frac{1}{\sqrt{N_{T}}}\left[1, e^{j\psi_{\ell}}, \cdots, e^{j(N_{T}-1)\psi_{\ell}}\right]^{T}. \tag{9}$$

From the prediction, the transceiver will get the estimation of AoA and AoD. The orientation of the beamformer is set as the estimated angle. By representing the orientation of the combiner and beamformer by $\overline{\psi}_{\ell}$, the directional beamformer can be represented as:

$$\mathbf{w}\left(\overline{\psi}_{\ell}\right) = \frac{1}{\sqrt{N_{R}}}\left[1, e^{j\overline{\psi}_{\ell}}, \cdots, e^{j(N_{R}-1)\overline{\psi}_{\ell}}\right]^{T}. \tag{10}$$

$$\mathbf{f}\left(\overline{\psi}_{\ell}\right) = \frac{1}{\sqrt{N_{T}}}\left[1, e^{j\overline{\psi}_{\ell}}, \cdots, e^{j(N_{T}-1)\overline{\psi}_{\ell}}\right]^{T}. \tag{11}$$

Finally, the observed signal can be represented as:

$$r_{\ell} = \sqrt{\rho_{\ell}}\beta_{\ell}\mathbf{w}^{H}\left(\overline{\psi}_{\ell}\right)\mathbf{a}_{R}\left(\psi_{\ell}\right)\mathbf{a}_{T}^{H}\left(\psi_{\ell}\right)\mathbf{f}\left(\overline{\psi}_{\ell}\right)s + n_{\ell}. \tag{12}$$

As shown in Fig. 3, the RSU height is represented by h_{RSU}. At discrete time ℓ, the coordinates of vehicles in the moving direction (x-axis) are x_{ℓ}. The coordinates of vehicles to roadside direction (y-axis) of the RSU side are y_{ℓ}. There is a certain deflection angle φ in the vehicle forward, which represents the possible direction deviation in the vehicle driving process. The angle representing the beam direction in space is decomposed into the

azimuth angle of the horizontal plane and the pitch angle of the vertical plane, then the azimuth AoD and pitch AoD are respectively defined as:

$$\sin\theta_1 = x\left(x^2 + y^2\right)^{-\frac{1}{2}}.$$

(13)

$$\cos\theta_2 = \left(x^2 + y^2\right)^{\frac{1}{2}}\left(x^2 + y^2 + h_{RSU}^2\right)^{-\frac{1}{2}}.$$

(14)

Based on this scenario, ψ can be expressed by azimuth angle and pitch angle as:

$$\psi = \pi\sin\theta_1\cos\theta_2 = \pi x\left(x^2 + y^2 + h_{RSU}^2\right)^{-\frac{1}{2}}.$$

(15)

3 Threshold Prediction Updated EKF Beam Tracking

3.1 Beam Tracking Procedure

Aiming at the problem of RSU downlink tracking vehicle users in mmWave IoV scenarios, this paper proposes an EKF algorithm based on threshold prediction update. The overall process of the beam tracking is displayed in Fig. 5. As described in the scenario model above, IoV users constantly broadcast their status information to RSU and users in the coverage area. Therefore, it can be considered that RSU can obtain the vehicle status information at the last moment in the algorithm. To highlight main study points, we suppose that the communication link has been established to facilitate the attention to the following beam tracking.
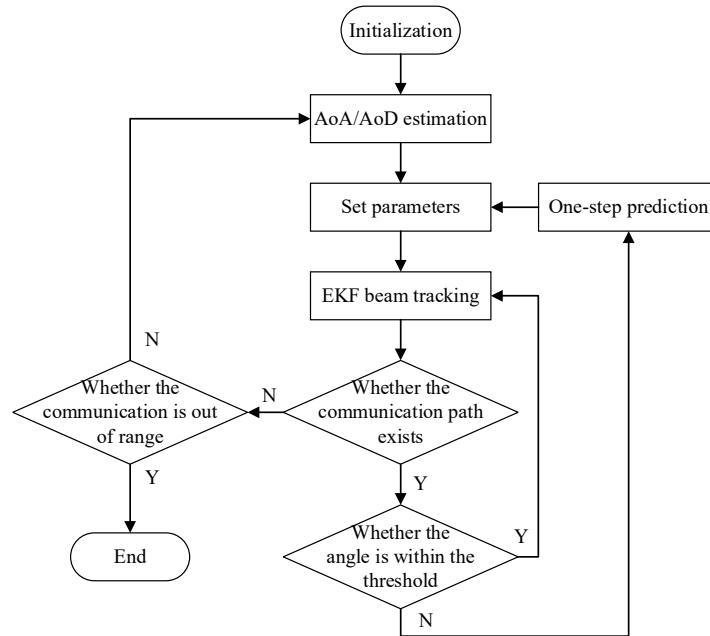
Fig. 5. Flow chart of beam tracking process

The initialization of the parameters is performed first, and estimation of angles is performed to build the connectivity, and constant beam tracking is then implemented using the EKF algorithm. There are five iterative steps

in the EKF process, with the predictive process in the first two steps and the corrective procedure in the subsequent three steps. The fundamental concept is to neutralize the nonlinear system by Taylor expansion and then apply KF. The shortcoming is that linearization generates a consequent accumulation of linear errors. Vehicle users are limited by roads, transportation situations and transportation regulations in IoV scenarios, and the vehicle movement trajectories are somewhat regulated and easy to predict, making the EKF can be well applied in this scenario. The EKF algorithm can realize two kinds of accuracy estimation: first-order Taylor expansion and second-order Taylor expansion. Higher-order expansions have greater precision, but also larger complexity. Given the demand for low latency in the IoV scenario, we adopt only the first-order Taylor expansion method to perform the estimation for the sake of reducing the computational complexity. Since the EKF algorithm approaches a nonlinear procedure to a linear one for estimation, estimation errors will inevitably be generated. With the advance of time, this error will be rapidly accumulated, which will lead to the decrease of tracking accuracy, resulting in a sharp decline in tracking accuracy or even break in communication. Hence, a check system needs to be added to keep correcting the beam orientation. Firstly, it detects whether the path exists or not at regular intervals. If the path doesn't exist then check whether the user has left the coverage area of the RSU. If yes then end the communication of this RSU, otherwise re-estimate and establish a new link. In case the path is existing, the beam angle is checked to see if the beam angle is inside the pre-defined threshold. If within the scope then EKF beam tracking is continued. Otherwise, it will use the known information to make one-step prediction, correct the tracking variable, and then carry out EKF beam tracking. Normally, the range of threshold values should make the absolute difference in beam angle smaller or equal to half beam width. This ensures excellent transmission performance and allows room for beam adjustment. It does not accumulate a lot of errors during the beam adjustment process and lead to disconnected communication. The consistency and reliability of the beam tracking can be better guaranteed under this circumstance.

3.2 EKF Beam Tracking

This section describes complete steps of EKF beam tracking step in Fig. 5. The position coordinates x_ℓ, y_ℓ and velocity v_ℓ at discrete time ℓ are used as tracking objects. The status observation vector $\mathbf{t}_\ell$ is given by:

$$\mathbf{t}_\ell = \left[x_\ell, y_\ell, v_\ell \right]^{\mathrm{T}} . \qquad (16)$$

It should be noted that the state observation vector $\mathbf{t}_0 = [x_0, y_0, v_0]^{\mathrm{T}}$ at the initial time is regarded as having been acquired by the RSU.

The state space equation of the system can be expressed as:

$$\mathbf{t}_\ell = \mathbf{S}\mathbf{t}_{\ell-1} + \mathbf{w}_{\ell-1} . \qquad (17)$$

This equation represents the actual change of the state observation vector, where $\mathbf{w}_{\ell-1} \sim \mathcal{CN}(0, \mathbf{Q}_\omega)$ represents noise motivation vector on discrete time $\ell - 1$. According to the change model of state variables, the state transition matrix $\mathbf{S}$ can be expressed as:

$$\mathbf{S} = \begin{bmatrix} 1 & 0 & T_s \cos\varphi \\ 0 & 1 & T_s \sin\varphi \\ 0 & 0 & 1 \end{bmatrix} . \qquad (18)$$

The process noise matrix $\mathbf{Q}_\omega$ in the noise excitation vector is denoted as:

$$\mathbf{Q}_\omega = diag\left[T_s^2 \sigma_\omega^2 \cos^2\varphi, T_s^2 \sigma_\omega^2 \sin^2\varphi, \sigma_\omega^2 \right] . \qquad (19)$$

Where φ is the vehicle deflection angle. Considering the actual situation, its value range is $[-\pi/2, \pi/2]$, T_s is the step in discrete time ℓ, and σ_ω^2 is the variance of the error parameter.

Taking the received signal r_ℓ as the system measurement equation, (12) can be re-expressed as:

$$r_\ell = \mathbf{h}(\psi_\ell) + n_\ell . \tag{20}$$

In actual calculation, the real and imaginary parts need to be calculated separately, so (20) can be rewritten as:

$$\tilde{\mathbf{r}}_\ell = \tilde{\mathbf{h}}(\psi_\ell) + \tilde{\mathbf{n}}_\ell . \tag{21}$$

All the variables included in (21) are expressed in real field as;

$$\tilde{\mathbf{r}}_\ell = \left[r_\ell^{re}, r_\ell^{im} \right]^\mathrm{T} . \tag{22}$$

$$\tilde{\mathbf{h}}(\psi_\ell) = \left[\mathbf{h}^{re}(\psi_\ell), \mathbf{h}^{im}(\psi_\ell) \right]^\mathrm{T} . \tag{23}$$

$$\tilde{\mathbf{n}}_\ell = \left[n_\ell^{re}, n_\ell^{im} \right]^\mathrm{T} . \tag{24}$$

The real and imaginary parts of the array response vector contained in (23) are respectively given by:

$$\mathbf{a}_R^{re}(\psi_\ell) = \left[\cos(0), \cos(\psi_\ell), \cdots, \cos((N_R - 1)\psi_\ell) \right]^\mathrm{T} . \tag{25}$$

$$\mathbf{a}_R^{im}(\psi_\ell) = \left[\sin(0), \sin(\psi_\ell), \cdots, \sin((N_R - 1)\psi_\ell) \right]^\mathrm{T} . \tag{26}$$

$$\mathbf{a}_T^{re}(\psi_\ell) = \left[\cos(0), \cos(\psi_\ell), \cdots, \cos((N_T - 1)\psi_\ell) \right]^\mathrm{T} . \tag{27}$$

$$\mathbf{a}_T^{im}(\psi_\ell) = \left[\sin(0), \sin(\psi_\ell), \cdots, \sin((N_T - 1)\psi_\ell) \right]^\mathrm{T} . \tag{28}$$

The detection process is linearized in order to carry out the EKF filtering process. According to (15), the function ψ_ℓ of beam direction is given as a function related to state vector at the moment of ℓ, namely:

$$\psi_\ell = \pi x_\ell \left(x_\ell^2 + y_\ell^2 + h_{RSU}^2 \right)^{-\frac{1}{2}} \doteq g(\mathbf{t}_\ell) . \tag{29}$$

In this case, (21) can be reformulated into:

$$\tilde{\mathbf{r}}_\ell = \tilde{\mathbf{h}}(g(\mathbf{t}_\ell)) + \tilde{\mathbf{n}}_\ell . \tag{30}$$

Then the received signal can be approximated by the predicted state vector $\hat{\mathbf{t}}_{\ell|\ell-1}$ at time ℓ through the first-order Taylor series, which is denoted as:

$$\tilde{\mathbf{r}}_\ell \simeq \tilde{\mathbf{h}}\left(g\left(\hat{\mathbf{t}}_{\ell|\ell-1}\right)\right) + \tilde{\mathbf{G}}_{\ell|\ell-1}\left(\mathbf{t}_\ell - \hat{\mathbf{t}}_{\ell|\ell-1}\right) + \tilde{\mathbf{n}}_\ell . \tag{31}$$

Where $\hat{\mathbf{t}}_{\ell|\ell-1}$ is the estimated value of the observation vector $\mathbf{t}_\ell$ at time $\ell - 1$, $\tilde{\mathbf{h}}\left(g\left(\hat{\mathbf{t}}_{\ell|\ell-1}\right)\right)$ is the predicted value of the Kalman state, $\tilde{\mathbf{G}}_{\ell|\ell-1}$ is the Jacobian matrix of the channel matrix, expressed as:

$$\tilde{\mathbf{G}}_{\ell|\ell-1} = \frac{\partial \mathbf{h}(g(\mathbf{t}))}{\partial \mathbf{t}}\bigg|_{\mathbf{t}=\hat{\mathbf{t}}_{\ell|\ell-1}} = \begin{bmatrix} \dot{\mathbf{h}}^{re}(g(\hat{\mathbf{t}}_{\ell|\ell-1})) \\ \dot{\mathbf{h}}^{im}(g(\hat{\mathbf{t}}_{\ell|\ell-1})) \end{bmatrix} \dot{g}(\hat{\mathbf{t}}_{\ell|\ell-1}). \tag{32}$$

The terms in (32) are respectively expressed as:

$$\dot{\mathbf{h}}^{re}(\psi_\ell) \doteq \frac{\partial \mathbf{h}^{re}(\psi)}{\partial \psi}\bigg|_{\psi=\psi_\ell}. \tag{33}$$

$$\dot{\mathbf{h}}^{im}(\psi_\ell) \doteq \frac{\partial \mathbf{h}^{im}(\psi)}{\partial \psi}\bigg|_{\psi=\psi_\ell}. \tag{34}$$

$$\dot{g}(\hat{\mathbf{t}}_{\ell|\ell-1}) \doteq \frac{\pi[\hat{y}_{\ell|\ell-1}^2 + h_{RSU}^2, -\hat{x}_{\ell|\ell-1}\ \hat{y}_{\ell|\ell-1}, \cos\varphi(\hat{y}_{\ell|\ell-1}^2 + h_{RSU}^2)]T_s}{(\hat{x}_{\ell|\ell-1}^2\ \hat{y}_{\ell|\ell-1}^2 + h_{RSU}^2)^{\frac{3}{2}}}. \tag{35}$$

Equation (35) can be approximated by the following process that:

$$\frac{\partial g(\mathbf{t})}{\partial \mathbf{t}} = \left[\frac{\partial g(\mathbf{t})}{\partial x}, \frac{\partial g(\mathbf{t})}{\partial y}, \frac{\partial g(\mathbf{t})}{\partial v}\right]\bigg|_{\mathbf{t}=[x,y,v]^{\mathrm{T}}}. \tag{36}$$

The approximated received signal, namely (31), is expanded as:

$$\tilde{\mathbf{r}}_\ell \simeq \tilde{\mathbf{G}}_{\ell|\ell-1}\mathbf{t}_\ell + \tilde{\mathbf{h}}(g(\hat{\mathbf{t}}_{\ell|\ell-1})) - \tilde{\mathbf{G}}_{\ell|\ell-1}\hat{\mathbf{t}}_{\ell|\ell-1} + \tilde{\mathbf{n}}_\ell. \tag{37}$$

In general, there are mainly five iterative steps in the EKF procedure, with the predictive procedure in the first two steps and the corrective procedure in the subsequent three steps. The nonlinear system is first approximated linearly and then processed using KF theory. The details are as follows:

1) State Prediction

$$\hat{\mathbf{t}}_{\ell|\ell-1} = \mathbf{S}\hat{\mathbf{t}}_{\ell-1|\ell-1}. \tag{38}$$

Where, $\mathbf{S}$ represents the status transfer matrix in (17).

2) Calculation of Prior Covariance Matrix

$$\mathbf{P}_{\ell|\ell-1} = \mathbf{S}\mathbf{P}_{\ell-1|\ell-1}\mathbf{S}^{\mathrm{T}} + \mathbf{Q}_\omega. \tag{39}$$

Where, the covariance matrix at time 0 is initialized as $\mathbf{P}_{0|0} = \sigma_\varepsilon^2(\mathbf{t}_0\mathbf{t}_0^{\mathrm{T}})$, σ_ε^2 is the variance of the initial feedback error parameter, and process noise matrix $\mathbf{Q}_\omega$ is shown in (19).

3) Kalman Gain Matrix Update

$$\mathbf{K}_\ell = \mathbf{P}_{\ell|\ell-1}\tilde{\mathbf{G}}_{\ell|\ell-1}^{\mathrm{T}}\left(\tilde{\mathbf{G}}_{\ell|\ell-1}\mathbf{P}_{\ell|\ell-1}\tilde{\mathbf{G}}_{\ell|\ell-1}^{\mathrm{T}} + \frac{\mathbf{I}_2}{2\rho_\ell}\right)^{-1}. \tag{40}$$

Where, $\mathbf{K}_\ell$ is the Kalman gain matrix in the KF process, and $\mathbf{I}$ is the identity matrix.

4) Update the Posterior Estimate of System State

$$\hat{\mathbf{t}}_{\ell|\ell} = \hat{\mathbf{t}}_{\ell|\ell-1} + \mathbf{K}_\ell(\tilde{\mathbf{r}}_\ell - \tilde{\mathbf{h}}(g(\hat{\mathbf{t}}_{\ell|\ell-1}))). \tag{41}$$

The result of this equation is the estimated value of the system we require, containing user coordinate and velocity information of the predicted discrete time ℓ.

5) Update the Posterior Covariance Matrix

$$\mathbf{P}_{\ell|\ell} = \left(\mathbf{I}_3 - \mathbf{K}_\ell \tilde{\mathbf{G}}_{\ell|\ell-1}\right)\mathbf{P}_{\ell|\ell-1}. \tag{42}$$

At this point, one iteration is complete, the parameters are updated to start a new round of iterations. However, because the EKF algorithm approximates the nonlinear systems as linear systems, each round of iterations will introduce a certain error. The error will accumulate with increasing number of iterations Therefore, it is essential to introduce a detecting mechanism to rectify the tracking process to limit this situation, increase the persistence and accuracy of beam tracking, and avoid the huge overhead caused by frequent channel estimation caused by poor communication quality or link disconnection.

As mentioned above, the half-beam width is used as the adjustment threshold, and the beam width is generally expressed as:

$$BW = \frac{0.886\lambda}{Md}. \tag{43}$$

Where λ indicates the signal wavelength, M represents the number of array elements, and d is the distance between adjacent antenna elements. It is worth noting that the antenna interval is generally set as $d = \lambda/2$ in the MIMO system.

According to (15), the state vector iterated by EKF algorithm is used to calculate the pointing angle $\hat{\psi}_\ell$. If it exceeds the threshold, that is:

$$\left|\hat{\psi}_\ell - \overline{\psi}_\ell\right| \geq BW/2. \tag{44}$$

Then the state information at the previous time is used for one-step prediction:

$$\hat{x}_{\ell|\ell} = x_{\ell-1} + v_{\ell-1}T_s\cos\varphi. \tag{45}$$

$$\hat{y}_{\ell|\ell} = y_{\ell-1} + v_{\ell-1}T_s\sin\varphi. \tag{46}$$

$$\hat{v}_{\ell|\ell} = v_{\ell-1}. \tag{47}$$

At the end of each iteration, the detection mechanism is introduced to correct the state variable beyond the threshold to the above value, and then the next round of EKF iteration is carried out.

4 Simulation

This chapter presents a simulation analysis of the beam tracking algorithm in the 3D scene proposed in this paper. The MSE is used as the performance index of tracking error. The tracking performance difference between the proposed algorithm and other existing algorithms and the performance of the proposed algorithm in various conditions are compared. The ULA-based MIMO system is adopted, and the default antenna interval is $d = \lambda/2$. Consider the system with center frequency $f_c = 28\text{GHz}$ and bandwidth $B = 20\text{MHz}$. Based on this, the noise power over a given bandwidth can be calculated as:

$$\sigma_n^2 = -174 + 10\lg(20\times10^6) \simeq -101\text{dBm}. \tag{48}$$

Given that the path loss index as $n = 2$, the time slot period size as $T_s = 10$ms, the initial position coordinate of the vehicle is initialized to (−50m, 8.5m), and the RSU height is set as $h_{\mathrm{RSU}} = 20$m. Assuming that the error parameter follows Gaussian distribution, the standard deviation of the error parameter is given as $\sigma_\omega = 10^{-1.5}$. Similarly, the standard deviation of the initial feedback error parameter is given as $\sigma_\varepsilon = 10^{-1.5}$. The reference power gain factor was normalized to $\tilde{\beta} = 1$. If there is no special comparison, the default antenna number for both transmitter and receiver is 16, the transmission power is −20dBm, the deflection angle of vehicle motion is $\pi/2^7$, and the initial velocity of vehicle motion is 10m/s. Table 1 lists the preceding public simulation parameters.

Table 1. Simulation parameters

Parameter	Value
f_c	28GHz
B	20MHz
σ_n^2	−101dBm
n	2
T_s	10ms
(x_0, y_0)	(−50m, 8.5m)
h_{RSU}	20m
σ_ω	$10^{-1.5}$
σ_ε	$10^{-1.5}$
$\tilde{\beta}$	1
N_T	16
N_R	16
p	−20dBm
φ	$\pi/2^7$
v_0	10m/s

Fig. 6 compares the tracking MSE of the algorithm in [14] and [19] with the algorithm in this paper. The method in [14] is the EKF algorithm of half-beam threshold adjustment based on the angle and gain tracking model. Reference [19] is an EKF algorithm in two-dimensional scenarios with distance, speed and gain as tracking variables. Due to the different tracking models adopted, in order to visually observe their MSE performance gap, the tracking coordinates in this paper are converted into beam angles, and then compared with these two algorithms. As shown in Fig. 6, the tracking errors of several algorithms are gradually increasing. This is because of the inevitable linearization error introduced in the EKF algorithm, which is continuously accumulated with each round of iteration. The tracking error of the scheme in [14] is the largest, which further validates the view in [19] that the new state evolution and observation model based on position and velocity is more practical for V2I communication. Compared with the other two algorithms in the figure, the simulation curve MSE of the proposed algorithm is lower, the tracking accuracy is higher, and the stable communication time is longer.
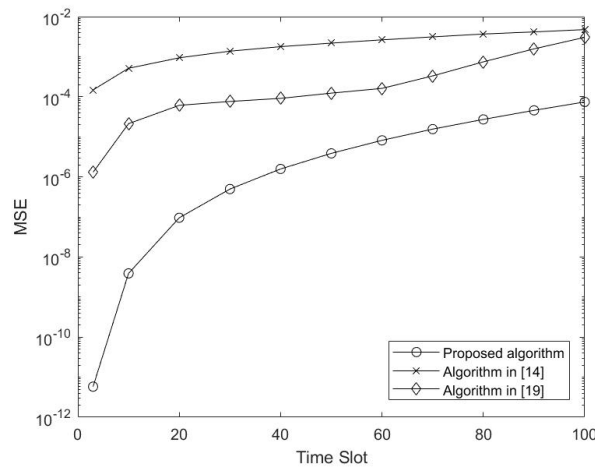
Fig. 6. Performance comparison of several tracking algorithms

Fig. 7 compares the MSE performance of the x-coordinate with that of the y-coordinate for the simulation. It can be seen that the MSE of the y-coordinate is much smaller than that of the x-coordinate, and the initial error of the y-coordinate is also lower, and the MSE performance of both tends to smooth out as the number of iteration rounds increases. And the tracking error of y-coordinate increases more slowly in the late iteration to time. This is because the main forward direction of the vehicle is the x-axis direction, and the movement on the y-axis is due to the presence of a deflection of the travel direction, but this movement is smaller, resulting in a much smaller tracking error in the y-coordinate than in the x-coordinate. In addition, it is worth mentioning that in Fig. 7 compared with Fig. 6, it can be clearly observed that the MSE reflected on the coordinates under the same algorithm is larger than that reflected on the angles. this is because the MSE of the angles will not be equally reflected on the coordinates, although the angular deviation is smaller, but we can know from the geometric principle that the same angular deviation, with the increase of the mapping distance, the more deviation will be fed back to the coordinates the deviation of the same angle will be larger as the mapping distance increases. The higher the height of the RSU, the greater the distance between the transceiver and the transmitter, so that the smaller angular error is reflected in the coordinates. For the sake of simplicity and intuition of the subsequent simulation, only the x-coordinate, which has a larger tracking error and is the main forward direction, is used for the next simulation.
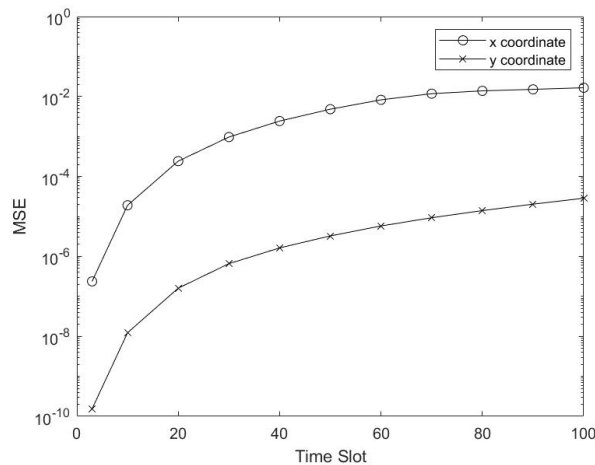
Fig. 7. Performance comparison of tracking algorithm between x coordinate and y coordinate

Fig. 8 compares the MSE performance of the algorithms in this paper over time under different antenna numbers. It is observed from the figure that, with different number of antennas, the MSE shows an increasing trend with the advance of time. That is because of the accumulated error brought by the EKF algorithm linearizing the nonlinear system in each round of iterations. The comparison shows that the tracking error is larger when the number of antennas is 8 and smaller when the number of antennas is 32. That is, a larger number of antennas will have a smaller tracking error. This conforms to the law that the more antennas, the more reliable the communication beam. However, it is important to note that the larger the number of antennas, the better. The increase in the number of antennas on the one hand will increase the cost of the device, on the other hand will make the beamwidth of the beamforming narrower. The narrower the beam is also more difficult to align in practice, and a slight Angle deviation may lead to a sharp decline in communication performance. Therefore, the selection of the number of antennas at the receiving and sending end needs to proceed from the actual situation, and select a proper compromise number.

Fig. 9 compares the influence of different transmission power on the algorithm in this paper, and the transmission power is p in (4). By analyzing the curves in the figure, it can be seen that different transmission power still conforms to the increasing trend of error accumulation of EKF algorithm, and the higher the transmission power, the smaller the tracking error. The two curves with transmission power of -40dBm and -60dBm almost coincide. After amplification, it can be observed that the curve with transmission power of -60dBm has a large tracking error, which conforms to the above law. The difference between the two is small because the transmission power of the two is already small, and the influence of noise is relatively close. According to (4), it can be seen that the

two transmission powers have close SNR. The effect shown in this simulation diagram conforms to the basic physical law that the larger the SNR, the smaller the tracking error.
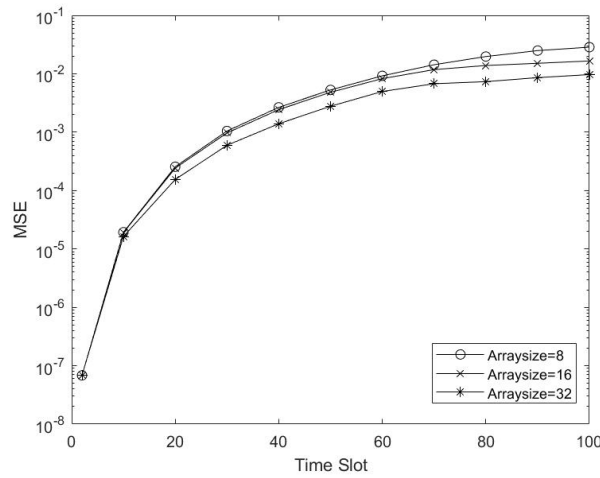
Fig. 8. Performance comparison of tracking algorithm with different number of antennas
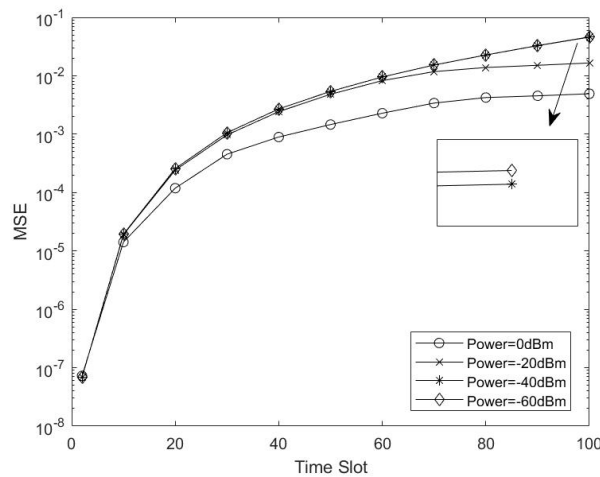
Fig. 9. Performance comparison of tracking algorithm with under different transmission power

The tracking error curves for the three deflection angles almost coincide with each other in Fig. 10. The reasons for this situation have been mentioned above. The deflection angles applied here are small, and the main direction of travel is the x-axis. Only a slight deflection in the driving direction is considered, so the influence of different deflection angles on the tracking error is very small. After enlarging the curve locally, it can be observed that the larger the deflection angle is, the smaller the tracking error will be. The smaller the deflection angle is, the larger the tracking error will be. This is because with the same forward speed, the larger the deflection angle, the smaller the speed component in x-axis orientation, and the smaller the tracking error. The smaller the deflection angle, the larger the speed component in x-axis orientation, and the larger the tracking error. This is consistent with the physics law that the faster the speed, the worse the tracking effect. It should be noted that the law of the deflection angle reflected in the tracking error is opposite to the x-axis direction in the y-axis direction. When the deflection angle is large, the velocity component on the y-axis will be larger and the tracking error will be larger. When the deflection angle is small, the velocity component on the y-axis will be smaller and the tracking error will be smaller.
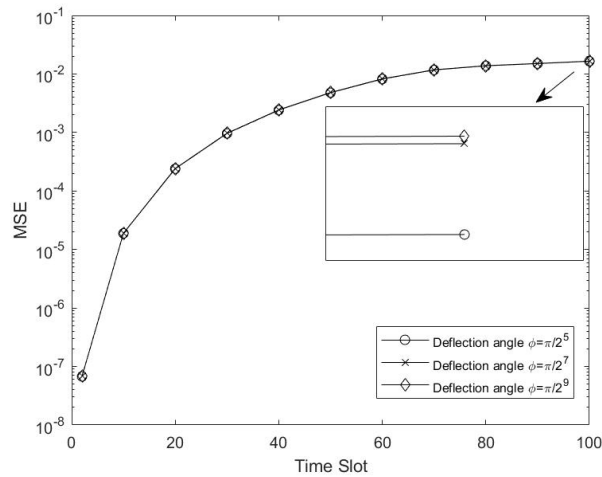
Fig. 10. Performance comparison of tracking algorithm under different deflection angles

Fig. 11 compares the tracking error at different initial velocities. It can be seen that when the speed is 5m/s, 10m/s, 15m/s, it is consistent with the performance that the faster the speed is, the larger the tracking error is, and the faster the movement speed is, the more difficult it is to improve the tracking. But when the speed is 20m/s, 25m/s, the tracking error instead tends to slow down the growth or even decrease after a certain time, and the trend of decrease is greater on the side of greater speed. This is because the speed is faster, and in this simulation the vehicle user approaches the RSU at a higher speed, and the spatial distance from the RSU is smaller in the same time compared to the slower speed. According to equation (4), a smaller spatial distance will have a higher SNR, and the increasing SNR will suppress or even reduce the tracking error as the vehicle approaches the RSU quickly. As mentioned earlier, the tracking error of the coordinates is also affected by the distance between the user and the RSU, the closer the distance to the RSU the higher the SNR will be, and the coordinates will have a smaller MSE. and if the RSU height is lower, with the further reduction of the spatial distance between the transceiver and the transmitter SNR will further increase, then the lower speed will also show a tendency to decrease the error earlier. In contrast, if the vehicle is not heading towards the RSU but away from it, a greater travel speed will conversely give the user a greater estimation error.
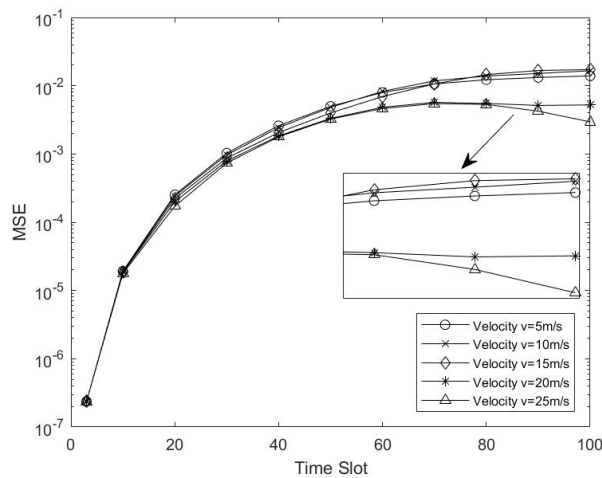
Fig. 11. Performance comparison of tracking algorithms with different initial velocities

5 Conclusion

This paper proposes an EKF-based tracking algorithm with threshold prediction update is proposed for the millimeter wave IoV scenario to implement constant and reliable beam tracking by overcoming the complicated channel conditions and the limitations arising from millimeter wave features. Due to the high complexity, inapplicability and incompatibility of the classical state model of gain and angle tracking to the mmWave IoV, a state tracking model based on vehicle position coordinates and velocity is adopted, and the occlusion effect and driving angle deflection are comprehensively considered. The 3D system model based on MIMO is derived and implemented, and the performance of the algorithm under the system model is simulated with MSE as the performance index. The simulation results demonstrate that the proposed algorithm has better performance than the tracking algorithm with angle and gain, with lower tracking error than existing algorithms, and can implement constant and steady beam tracking. Moreover, compared with the position velocity model discussed only in the 2D case, it considers possible realistic situations, and has more practical significance. Nevertheless, this paper doesn't consider the situation of antenna arrays that may be used besides the ULA and the actual road conditions of the vehicle driving on the slope. The subsequent work can be further studied for the contents mentioned above.

6 Acknowledgement

References

[1] J. Hu, C. Chen, T. Qiu, Q. Pei, Regional-Centralized Content Dissemination for eV2X Services in 5G mmWave-Enabled IoV, IEEE Internet of Things Journal 7(8)(2020) 7234-7249.

[2] D. Moltchanov, R. Kovalchukov, M. Gerasimenko, S. Andreev, Y. Koucheryavy, M. Gerla, Socially Inspired Relaying and Proactive Mode Selection in mmWave Vehicular Communications, IEEE Internet of Things Journal 6(3)(2019) 5172-5183.

[3] Y. Cao, X. He, C. Yu, C. Yin, Reliability and Latency of MmWave Communications Based on Blockage Avoidance in Internet of Vehicles, in: Proc. 2021 13th International Conference on Wireless Communications and Signal Processing (WCSP), 2021.

[4] D. Kwon, J. Kim, D.A. Mohaisen, W. Lee, Self-adaptive power control with deep reinforcement learning for millimeter-wave Internet-of-vehicles video caching, Journal of Communications and Networks 22(4)(2020) 326-337.

[5] K.Z. Ghafoor, L. Kong, S. Zeadally, A.S. Sadiq, G. Epiphaniou, M. Hammoudeh, A.K. Bashir, S. Mumtaz, Millimeter-Wave Communication for Internet of Vehicles: Status, Challenges, and Perspectives, IEEE Internet of Things Journal 7(9)(2020) 8525-8546.

[6] J. Tan, L. Dai, Wideband beam tracking in THz massive MIMO systems, IEEE Journal on Selected Areas in Communications 39(6)(2021) 1693-1710.

[7] S. Blandino, J. Senic, C. Gentile, D. Caudill, J. Chuang, A. Kayani, Markov Multi-Beamtracking on 60 GHz Mobile Channel Measurements, IEEE Open Journal of Vehicular Technology 3(2021) 26-39.

[8] S.H. Lim, S. Kim, B. Shim, J.W. Choi, Deep learning-based beam tracking for millimeter-wave communications under mobility, IEEE Transactions on Communications 69(11)(2021) 7458-7469.

[9] B. Ning, Z. Chen, Z. Tian, C. Han, S. Li, A unified 3D beam training and tracking procedure for terahertz communication, IEEE Transactions on Wireless Communications 21(4)(2022) 2445-2461.

[10] L. Yang, W. Zhang, Beam tracking and optimization for uav communications, IEEE Transactions on Wireless Communications 18(11)(2019) 5367-5379.

[11] H.L. Song, Y.C. Ko, J. Cho, C. Hwang, Beam Tracking Algorithm for UAV Communications Using Kalman Filter, in: Proc. 2020 International Conference on Information and Communication Technology Convergence (ICTC), 2020.

[12] G.L. Liu, H.G. Duan, J.Z. Hou, Beam tracking based on second-order extended Kalman filter theory in millimeter wave communication systems, Journal of Chongqing University of Posts and Telecommunications (Natural Science Edition) 33(3)(2021) 412-419.

[13] C. Zhang, D. Guo, P. Fan, Tracking angles of departure and arrival in a mobile millimeter wave channel, in: Proc. 2016

IEEE International Conference on Communications (ICC), 2016.

[14] V. Va, H. Vikalo, R.W. Heath, Beam tracking for mobile millimeter wave communication systems, in: Proc. IEEE Global Conference on Signal and Information Processing (GlobalSIP), 2016.

[15] X. Xin, Y. Yang, Research on Extended Kalman Filter algorithm for millimeter wave beam tracking, Journal of Microwaves 35(6)(2019) 16-20.

[16] Y. Ge, Z. Zeng, T. Zhang, Y. Sun, Unscented Kalman Filter Based Beam Tracking for UAV-enabled Millimeter Wave Massive MIMO Systems, in: Proc. 2019 16th International Symposium on Wireless Communication Systems (ISWCS), 2019.

[17] S.G. Larew, D.J. Love, Adaptive beam tracking with the unscented kalman filter for millimeter wave communication, IEEE Signal Processing Letters 26(11)(2019) 1658-1662.

[18] J. Lim, H.M. Park, D. Hong, Beam Tracking under Highly Nonlinear Mobile Millimeter-Wave Channel, IEEE Communications Letters 23(3)(2019) 450-453.

[19] S. Shaham, M. Ding, M. Kokshoorn, Z. Lin, S. Dang, R. Abbas, Fast Channel Estimation and Beam Tracking for Millimeter Wave Vehicular Communications, IEEE Access 7(2019) 141104-141118.

[20] S.-H. Hyun, J. Song, K. Kim, J.-H. Lee, S.-C. Kim, Adaptive Beam Design for V2I Communications Using Vehicle Tracking with Extended Kalman Filter, IEEE Transactions on Vehicular Technology 71(1)(2022) 489-502.

[21] A.A. Farid, M. Abdelghany, U. Madhow, M.J.W. Rodwell, Dynamic Range Requirements of Digital vs. RF and Tiled Beamforming in mm-Wave Massive MIMO, in: Proc. 2021 IEEE Radio and Wireless Symposium (RWS), 2021.

[22] Y. Liu, Y. Hou, J. Wei, Y. Zhang, J. Zhang, T. Zhang, Joint Beam Selection and Precoding Based on Differential Evolution for Millimeter-Wave Massive MIMO Systems, in: Proc. ICASSP 2022 - 2022 IEEE International Conference on Acoustics, Speech and Signal Processing (ICASSP), 2022.

[23] F. Liu, W. Yuan, C. Masouros, J. Yuan, Radar-Assisted Predictive Beamforming for Vehicular Links: Communication Served by Sensing, IEEE Transactions on Wireless Communications 19(11)(2020) 7704-7719.